



HAL
open science

Copper Iodide Clusters Coordinated by Emissive Cyanobiphenyl-Based Ligands

Raquel Utrera-Melero, Florian Massuyeau, Camille Latouche, Franck
Camerel, Sandrine Perruchas

► **To cite this version:**

Raquel Utrera-Melero, Florian Massuyeau, Camille Latouche, Franck Camerel, Sandrine Perruchas. Copper Iodide Clusters Coordinated by Emissive Cyanobiphenyl-Based Ligands. *Inorganic Chemistry*, 2022, 61 (9), pp.4080-4091. 10.1021/acs.inorgchem.1c03876 . hal-03594145

HAL Id: hal-03594145

<https://hal.science/hal-03594145>

Submitted on 7 Jul 2022

HAL is a multi-disciplinary open access archive for the deposit and dissemination of scientific research documents, whether they are published or not. The documents may come from teaching and research institutions in France or abroad, or from public or private research centers.

L'archive ouverte pluridisciplinaire **HAL**, est destinée au dépôt et à la diffusion de documents scientifiques de niveau recherche, publiés ou non, émanant des établissements d'enseignement et de recherche français ou étrangers, des laboratoires publics ou privés.

Copper iodide clusters coordinated by emissive cyanobiphenyl-based ligands

Raquel Utrera-Melero,^a Florian Massuyeau,^a Camille Latouche,^{a} Franck Camerel,^{b*} and Sandrine Perruchas^{a*}*

^a Université de Nantes, CNRS, Institut des Matériaux Jean Rouxel, IMN, F-44000 Nantes, France.
Phone: (+33) (0)2 40 37 63 35. E-mail: camille.latouche@cncs-immn.fr, sandrine.perruchas@cncs-immn.fr

^b Laboratoire Matière Condensée et Systèmes Électroactifs (MaCSE), Institut des Sciences Chimiques de Rennes, UMR 6226 CNRS-Université de Rennes 1, Campus de Beaulieu, 35042 Rennes, France.
Email: fcamerel@univ-rennes1.fr

Abstract.

Copper(I) halides are currently the subject of intensive research because of their rich photophysical properties combined with economic and eco-friendly advantages for practical applications. The molecular copper iodide cluster of general formula $[\text{Cu}_4\text{I}_4\text{L}_4]$ (L = ligand) is a well-known photoluminescent compound, and the possibility to enlarge the panel of its photophysical properties is studied here, by exploring ligands bearing a distinct emitter. The comparative study of five copper iodide clusters coordinated by different phosphine ligands functionalized by the emissive cyanobiphenyl (CBP) group, is thus described in this work. The emissive properties of the ligands have a great impact onto the photophysical properties of the cluster. Compared with classical $[\text{Cu}_4\text{I}_4\text{L}_4]$ copper iodide clusters, the origin of the emission bands is largely modified. The CBP moiety of electron acceptor character significantly lowers in energy the vacant orbitals and consequently affects the global energetic layout. These clusters present dual emission based on two different emissive centers which interplay through energy transfer. This study demonstrates that the design of original ligands is an effective approach to enrich the photophysical properties of the appealing family of copper halide complexes.

Keywords. Copper iodide cluster, Cyanobiphenyl, Photoluminescence, Dual-emission, DFT.

Introduction

Luminescent materials present a wide range of applications in light-emitting devices and in the broad field of detection. In the course of rare-earth and lead-free phosphors in regards to economic and sustainable issues,¹⁻⁶ copper(I) halide complexes are emerging as serious candidates owing to their extremely rich optical properties.⁷⁻⁹ In fact, the great structural diversity of copper halides due to the d^{10} flexible electronic configuration of Cu(I) and the multiple connectivity modes of halides, lead to a extremely large panel of photophysical properties.¹⁰⁻¹⁶ Their potential applications as sensors,¹⁷⁻¹⁹ photocatalytic systems,²⁰ and emitters in organic light-emitting diodes (OLEDs),²¹⁻²⁵ have indeed been reported, featuring appealing perspectives that may well outperform the trendy hybrid perovskites.

A stand out Cu(I) halide complex, is the molecular cubane cluster formulated $[\text{Cu}_4\text{I}_4\text{L}_4]$ (L = organic ligand). Its outstanding stimuli-responsive photoluminescent properties ranging from luminescence thermochromism,²⁶⁻³¹ mechanochromism,³² solvatochromism³³⁻³⁶ to rigidochromism,³⁷⁻³⁹ are particularly appealing to access original multifunctional materials. Promising perspectives of applications have been already demonstrated with the development of inks based on $[\text{Cu}_4\text{I}_4\text{L}_4]$ clusters⁴⁰ and phosphors⁴¹ or emitters for lighting devices.^{42,43} The cubane structure of this copper iodide cluster is built on four copper atoms and four iodide atoms which alternatively occupy the vertices of a distorted cube. The ligands complete the four-fold tetrahedral coordination sphere of the copper(I) atoms.⁴⁴ Main studied ligands are nitrogen, phosphorus or sulfur-based ones. When the ligands bear aromatic substituents, additional luminescence features take place because of the presence of vacant π^* orbitals. Indeed, the luminescence thermochromic properties of these clusters involves such π^* -based transitions prevailing at low temperature.^{28,45,46} In the case of phosphine ligands, the PPh_2R (R = alkyl or aryl group) skeleton have been mainly studied,⁴⁷ but ligands bearing an emissive moiety have been barely reported.⁴⁸ Grafting an emissive center to the cluster could modify its photoluminescence properties by either a simple addition of an emissive transition or by fully modifying the global energetically layout. In either way, this strategy should enlarge the panel of photoluminescence properties displayed by these compounds.

During our previous investigations regarding the synthesis of metallomesogens based on copper iodide clusters, a phosphine ligand bearing CBP (cyanobiphenyl) groups was actually designed.⁴⁸ The CBP moiety commonly used in liquid crystals chemistry, is known to be photoluminescent and thus represents an emissive center by itself. The corresponding functionalized cubane cluster displayed original optical properties by exhibiting luminescence mechanochromism with a dual emissive feature. These attractive emission properties which presented different features compared with those of more classical copper iodide clusters were not rationalized. This preliminary work, motivated further investigations regarding the association of the $[\text{Cu}_4\text{I}_4\text{L}_4]$ cluster with CBP-based ligands.

Here, is reported the comparative study of five copper iodide clusters functionalized by different CBP-based phosphine ligands. The synthesis of these original ligands and corresponding clusters is described. The effect of the number of the emissive CBP groups born by the ligands and their spacing between the triphenylphosphine moiety, onto the photophysical properties of the clusters was evaluated. The CBP group affects the luminescence properties of the clusters by bringing additional emission bands which can be correlated to those of the $[\text{Cu}_4\text{I}_4]$ cluster core. The results of DFT calculations are discussed and shed light on this CBP-cluster photoactive system.

Experimental Section.

Synthesis. All synthetic manipulations were performed under inert and dry nitrogen atmosphere using standard techniques. Solvents were distilled from appropriate drying agents and degassed prior to use. The reactions were followed by Thin Layer Chromatography (TLC) plates, revealed with a UV-lamp at 254 nm. All reactants, CuI (Aldrich), (4-cyano-4'-hydroxybiphenyl (fluorochem), 4-(diphenylphosphino)benzoic acid 97% (Aldrich), 2-Bromoethanol 95% (Aldrich), 10-Bromo-1-decanol >85.0%(GC) (TCI), 4-Pyrrolidinopyridine (4-ppy) 98% (Aldrich) were purchased from commercial source and used as received. 5-[[[(1,1-Dimethylethyl)dimethylsilyl]oxy]-1,3-benzenedicarboxylic acid ligand⁴⁹ and cluster **C1**⁴⁸ were synthesized as previously described.

4'-(2-hydroxyethoxy)-[1,1'-biphenyl]-4-carbonitrile. Cyanobiphenyl (1.0 g, 5.0 mmol) is dissolved with bromoethanol (0.83 g, 1.3 eq., 6.6 mmol) and K₂CO₃ (3.5 g, 5eq., 25 mmol) in 20 mL DMF and the mixture is stirred for 3 days at 90 °C under nitrogen. After evaporation of the solvent, the residue is dissolved in dichloromethane (50 mL) and the organic phase is washed with water (3x50 mL) and dried over MgSO₄. The product is then purified by flash column chromatography on silica using a gradient of solvent from 50/50 dichloromethane/ petroleum ether to pure dichloromethane. After removal of the solvent, the white product is recrystallized from dichloromethane by slow diffusion of petroleum ether (0.82 g, 67%). ¹H NMR (300 MHz, CDCl₃) δ 7.68 (q, *J* = 8.5 Hz, 4H), 7.62 – 7.48 (m, 2H), 7.14 – 6.95 (m, 2H), 4.17 (dd, *J* = 5.2, 3.8 Hz, 2H), 4.03 (dd, *J* = 5.2, 3.8 Hz, 2H).

4'-((10-bromodecyl)oxy)-[1,1'-biphenyl]-4-carbonitrile. Cyanobiphenyl (2.74 g, 14 mmol), 10-Bromo-1-decanol (4 g, 1.2 eq., 17 mmol) and K₂CO₃ (9.7 g, 5 eq., 70 mmol) are dissolved in 30 mL DMF and the mixture is stirred for 3 days at 80 °C under nitrogen. After evaporation of the solvent, the product is purified by column chromatography on silica gel using a mixture of dichloromethane with 10 % ethyl acetate as eluent. After removal of the solvent, the product is isolated as a white powder (2.95 g, 60 %). ¹H NMR (300 MHz, CDCl₃) δ 7.75 – 7.59 (m, 4H), 7.59 – 7.45 (m, 2H), 7.07 – 6.92 (m, 2H), 4.00 (t, *J* = 6.5 Hz, 2H), 3.64 (t, *J* = 6.6 Hz, 2H), 1.93 – 1.69 (m, 2H), 1.68 – 1.18 (m, 14H).

Bis(2-((4'-cyano-[1,1'-biphenyl]-4-yl)oxy)ethyl) 5-((tert-butyldimethylsilyl)oxy)isophthalate. A solution of cold dichloromethane solution (20 mL) containing 5-[[[(1,1-Dimethylethyl)dimethylsilyl]oxy]-1,3-benzenedicarboxylic acid (0.31 g, 1 mmol), 4-(Dimethylamino)pyridinium 4-toluenesulfonate (DPTS) (0.52 g, 1.7 mmol), DCC (0.97 g, 4.7 mmol) and a spatula tip of 4-Pyrrolidinopyridine (4-ppy) is added dropwise to a cold dichloromethane solution (20 mL) containing 4'-(2-hydroxyethoxy)-[1,1'-biphenyl]-4-carbonitrile (0.5 g, 2 mmol). The mixture is stirred at room temperature for 4 days under nitrogen. After reaction, the organic solution is washed with water (3 x 50 mL) and dried over MgSO₄. The compound is then purified by flash column chromatography on silica gel using a gradient of solvent from 50/50 dichloromethane/ petroleum ether to pure dichloromethane. The product is isolated as a colorless oil (0.455 g, 62 %). ¹H NMR (300 MHz, CDCl₃) δ 8.32 (t, *J* = 1.5 Hz, 1H), 7.74 – 7.59 (m, 10H), 7.57 – 7.46 (m, 4H), 7.09 – 6.98 (m, 4H), 4.79 – 4.64 (m, 4H), 4.45 – 4.30 (m, 4H), 0.98 (s, 9H), 0.22 (s, 6H).

Bis(2-((4'-cyano-[1,1'-biphenyl]-4-yl)oxy)ethyl) 5-hydroxyisophthalate. To a solution of bis(2-((4'-cyano-[1,1'-biphenyl]-4-yl)oxy)ethyl) 5-((tert-butyldimethylsilyl)oxy)isophthalate (0.34 g, 0.48 mmol) in 15 mL THF is added TBAF 1M in THF solution (530 μL, 1.1 eq., 0.53 mmol) and the mixture is stirred for 24 H at room temperature under N₂. After evaporation of the solvent, the product is directly purified by flash column chromatography on silica gel using a gradient of solvent from pure dichloromethane to dichloromethane with 5% methanol. The product is isolated as a white powder in 84 % (0.25 g). ¹H NMR (300 MHz, CDCl₃) δ 8.30 (t, *J* = 1.4 Hz, 1H), 7.77 – 7.56 (m, 10H), 7.58 – 7.48 (m, 4H), 7.09 – 6.99 (m, 4H), 5.68 (s, 1H), 4.78 – 4.66 (m, 4H), 4.43 – 4.33 (m, 4H).

L2. 4-cyano-4'-hydroxybiphenyl (0.096 g, 0.49 mmol) is added dropwise to a solution of DCC (0.202 g, 0.98 mmol), DMAP (0.06 g, 0.49 mmol) and of 4-(diphenylphosphino)benzoic acid (0.15 g, 0.49 mmol) in degassed dichloromethane (10 mL). The solution is stirred at room temperature overnight

under nitrogen. After filtration and solvent evaporation, the product is purified by flash chromatography on silica gel using a gradient of solvent from 50/50 dichloromethane/ petroleum ether to pure dichloromethane. After solvent evaporation and drying under vacuum, the ligand is obtained as white powder (0.17 g, Yield = 73 %).

^1H NMR (300 MHz, CDCl_3) δ 8.21 – 8.06 (m, 2H), 7.77 – 7.62 (m, 6H), 7.53 – 7.29 (m, 14H). ^{13}C NMR (75 MHz, CDCl_3) δ 165.01 (C=O), 151.55 (Cq), 145.61 (Cq), 144.94 (Cq), 137.13 (Cq), 136.16 (Cq), 136.02 (Cq), 134.31 (CH), 134.05 (CH), 133.60 (CH), 133.36 (CH), 132.82 (CH), 130.07 (CH), 129.98 (CH), 129.45 (CH), 129.20 (Cq), 128.97 (CH), 128.87 (CH), 128.57 (CH), 127.86 (CH), 122.57 (CH), 118.98 (Cq), 111.28 (Cq). ^{31}P NMR (121 MHz, CDCl_3) δ (ppm): -4.62. MALDI-TOF-MS: m/z = 484.1 ($[\text{M}+\text{H}]^+$). Anal. Calc. for $\text{C}_{32}\text{H}_{22}\text{NO}_2\text{P}$ (%): C 79.49, H 4.59, N 2.90. Found (%): C 79.03, H 4.57, N 3.25.

L3. A solution of 4'-(2-hydroxyethoxy)-[1,1'-biphenyl]-4-carbonitrile (0.17 g, 1.1 eq., 0.72 mmol), DMAP (0.08 g, 1 eq., 0.65 mmol) and 4-(diphenylphosphino)benzoic acid (0.2 g, 1 eq., 0.65 mmol) in 10 mL CH_2Cl_2 is degassed 30 min with N_2 . After adding the DCC (0.27 g, 2 eq., 1.3 mmol), the solution is stirred at room temperature for 3 days under nitrogen. After complete reaction, the organic solution is washed with water (3 x 10mL) and dried over MgSO_4 . After evaporation of the solvent, the product is then purified by flash chromatography on silica gel using a gradient of solvent from 50/50 dichloromethane/ petroleum ether to pure dichloromethane. The ligand is obtained as white powder (0.12 g, Yield = 35 %).

^1H NMR (300 MHz, CDCl_3) δ 7.99 (dd, J = 8.2, 1.5 Hz, 2H), 7.75 – 7.58 (m, 5H), 7.58 – 7.48 (m, 2H), 7.43 – 7.26 (m, 12H), 7.12 – 6.94 (m, 2H), 4.79 – 4.60 (m, 2H), 4.36 (t, J = 4.7 Hz, 2H). ^{13}C NMR (75 MHz, CDCl_3) δ 166.36 (C=O), 159.28 (Cq), 145.18 (Cq), 144.73 (Cq), 144.54 (Cq), 136.28 (Cq), 136.14 (Cq), 134.20 (CH), 133.93 (CH), 133.40 (CH), 133.15 (CH), 132.69 (CH), 132.18 (Cq), 129.78 (Cq), 129.58 (CH), 129.50 (CH), 129.29 (CH), 128.85 (CH), 128.76 (CH), 128.55 (CH), 127.26 (CH), 119.14 (Cq), 115.42 (CH), 110.38 (Cq), 66.28 (OCH_2), 63.37 (OCH_2). ^{31}P NMR (121 MHz, CDCl_3) δ (ppm): -4.91. MALDI-TOF-MS: m/z = 528.2 ($[\text{M}+\text{H}]^+$). Anal. Calc. for $\text{C}_{34}\text{H}_{26}\text{NO}_3\text{P}$, 2/3 H_2O (%): C 75.69, H 5.11, N 2.60. Found (%): C 75.28, H 4.92, N 3.14.

L4. A solution of 4'-((10-bromodecyl)oxy)-[1,1'-biphenyl]-4-carbonitrile (0.2 g, 1 eq., 0.57 mmol), DMAP (0.069 g, 1 eq., 0.57 mmol) and 4-(diphenylphosphino)benzoic acid (0.19 g, 1.1 eq., 0.63 mmol) in 10 mL CH_2Cl_2 is degassed 30 min with N_2 . After adding the DCC (0.235 g, 2 eq., 1.14 mmol), the solution is stirred at room temperature for 6 days under nitrogen. After reaction, the reaction mixture was evaporated on celite and the product is then purified by flash chromatography on silica gel using a gradient of solvent from pure petroleum ether to pure dichloromethane. The ligand is obtained as white powder (0.32 g, Yield = 88 %).

^1H NMR (300 MHz, CDCl_3) δ 8.07 – 7.91 (m, 2H), 7.75 – 7.57 (m, 4H), 7.59 – 7.48 (m, 2H), 7.43 – 7.28 (m, 12H), 7.09 – 6.90 (m, 2H), 4.32 (t, J = 6.6 Hz, 2H), 4.01 (t, J = 6.5 Hz, 2H), 1.89 – 1.69 (m, 4H), 1.69 – 1.21 (m, 12H). ^{13}C NMR (75 MHz, CDCl_3) δ 166.51 (C=O), 159.91 (Cq), 145.35 (Cq), 144.09 (Cq), 143.90 (Cq), 136.39 (Cq), 136.25 (Cq), 134.16 (CH), 133.90 (CH), 133.38 (CH), 133.13 (CH), 132.63 (CH), 131.32 (Cq), 130.52 (Cq), 129.40 (CH), 129.31 (CH), 129.22 (CH), 128.81 (CH), 128.72 (CH), 128.40 (CH), 127.14 (CH), 119.18 (Cq), 115.20, 110.13 (Cq), 68.24 (OCH_2), 65.25 (OCH_2), 29.55 (CH_2), 29.52 (CH_2), 29.42 (CH_2), 29.32 (CH_2), 29.30 (CH_2), 28.80 (CH_2), 26.11 (CH_2). ^{31}P NMR (121 MHz, CDCl_3) δ (ppm): -5.01. MALDI-TOF-MS: m/z = 640.4 ($[\text{M}+\text{H}]^+$). Anal. Calc. for $\text{C}_{42}\text{H}_{42}\text{NO}_3\text{P}$, 0.5 H_2O (%): C 77.76, H 6.68, N 2.16. Found (%): C 77.55, H 6.51, N 2.46.

L5. A solution of bis(2-((4'-cyano-[1,1'-biphenyl]-4-yl)oxy)ethyl) 5-hydroxyisophthalate (0.22 g, 1 eq., 0.37 mmol), DMAP (0.045 g, 1 eq., 0.65 mmol) and 4-(diphenylphosphino)benzoic acid (0.125 g, 1.1 eq., 0.41 mmol) in 10 mL CH_2Cl_2 is degassed 30 min with N_2 . After adding the DCC (0.155 g, 2 eq., 0.75 mmol), the solution is stirred at room temperature for 6 days under nitrogen. After complete reaction, the organic solution is directly evaporated on celite and the product is purified by flash

chromatography on silica gel using mixture of dichloromethane + 2% MeOH as eluent. The product is isolated as a white powder (0.12 g, Yield = 36 %).

^1H NMR (300 MHz, CDCl_3) δ 8.65 (t, $J = 1.5$ Hz, 1H), 8.14 – 8.05 (m, 4H), 7.72 – 7.57 (m, 8H), 7.57 – 7.47 (m, 4H), 7.46 – 7.29 (m, 12H), 7.09 – 6.98 (m, 4H), 4.78 – 4.68 (m, 4H), 4.42 – 4.33 (m, 4H). ^{13}C NMR (75 MHz, CDCl_3) δ 164.86 (C=O), 164.66 (C=O), 159.20 (Cq), 151.11 (Cq), 146.40 (Cq), 146.19 (Cq), 145.17 (Cq), 136.04 (Cq), 135.90 (Cq), 134.31 (CH), 134.04 (CH), 133.56 (CH), 133.31 (CH), 132.70 (CH), 132.30 (Cq), 131.99 (Cq), 130.04 (CH), 129.96 (CH), 129.47 (CH), 128.97 (CH), 128.87 (CH), 128.59 (Cq), 128.51 (Cq), 127.79 (CH), 127.28 (CH), 119.12 (Cq), 115.47 (CH), 110.45 (Cq), 66.10 (OCH_2), 64.01 (OCH_2), 53.54 (OCH_2). ^{31}P NMR (121 MHz, CDCl_3) δ (ppm): -4.55. MALDI-TOF-MS: $m/z = 913.4$ ($[\text{M}+\text{H}]^+$). Anal. Calcd. for $\text{C}_{57}\text{H}_{41}\text{N}_2\text{O}_8\text{P}$, 2(CH_3OH) (%): C 72.53, H 5.06, N 2.87. Found (%): C 72.43, H 4.93, N 3.06.

C2. To a CuI suspension (0.050 g, 0.26 mmol) in dichloromethane (20 mL), **L2** ligand (0.127 g, 0.26 mmol) is added. The yellow solution is stirred for 12 h. After filtration and evaporation of the solvent, the yellow pasty solid obtained is washed with diethyl ether. The product is obtained as a yellow solid with a yield of 34 %. ^1H NMR (400 MHz, CD_2Cl_2): δ (ppm) = 8.20-7.10 (m, Ph). ^{31}P NMR (121.5 MHz, CD_2Cl_2): δ (ppm) = -22.0. Anal. Calcd (% wt.) for $\text{C}_{128}\text{H}_{88}\text{O}_8\text{N}_4\text{P}_4\text{Cu}_4\text{I}_4$: C, 57.03; H, 3.29; N, 2.08. Found: C, 56.89; H, 3.22; N, 1.89.

C3. Same procedure as **C2** with CuI (0.060 g, 0.32 mmol), dichloromethane (20 mL), **L3** ligand (0.120 g, 0.23 mmol), yield 44 %. ^1H NMR (400 MHz, CDCl_3): δ (ppm) = 8.01-6.98 (m, 22H, Ph), 4.72 (t, 2H, CH_2), 4.38 (t, 2H, CH_2). ^{31}P NMR (121.5 MHz, CDCl_3): δ (ppm) = -21.7. Anal. Calcd (% wt.) for $\text{C}_{136}\text{H}_{104}\text{O}_{12}\text{N}_4\text{P}_4\text{Cu}_4\text{I}_4$: C, 56.88; H, 3.65; N, 1.95. Found: C, 56.22; H, 3.76; N, 1.64.

C4. Same procedure as **C2** with CuI (0.035 g, 0.187 mmol), dichloromethane (20 mL), **L4** ligand (0.120 g, 0.187 mmol), yield of 30 %. ^1H NMR (400 MHz, CDCl_3): δ (ppm) = 8.10-6.80 (22H, m, Ph), 5.22 (s, 2H, CH_2 Cl₂), 4.22 (s, 2H, CH_2), 3.89 (s, 2H, CH_2) 1.90-1.20 (m, 16H, CH_2) ^{31}P NMR (121.5 MHz, CDCl_3): δ (ppm) = -20.8. Anal. Calcd (% wt.) for $\text{C}_{168}\text{H}_{168}\text{O}_{12}\text{N}_4\text{P}_4\text{Cu}_4\text{I}_4$: C, 60.80; H, 5.10; N, 1.70. Found: C, 61.66; H, 5.42; N, 2.01.

C5. Same procedure as **C2** with CuI (0.080 g, 0.42 mmol), dichloromethane (30 mL), **L5** ligand (0.280 g, 0.31 mmol), yield of 65 %. ^1H NMR (400 MHz, CDCl_3): δ (ppm) = 8.60-6.97 (m, 33H, Ph), 4.73 (t, 4H, CH_2), 4.36 (t, 4H, CH_2). ^{31}P NMR (121.5 MHz, CDCl_3): δ (ppm) = -21.4. Anal. Calcd (% wt.) for $\text{C}_{228}\text{H}_{164}\text{O}_{32}\text{N}_8\text{P}_4\text{Cu}_4\text{I}_4$: C, 62.05; H, 3.75; N, 2.54. Found: C, 61.48; H, 4.01; N, 2.39.

Characterizations. ^1H , ^{13}C and ^{31}P NMR spectra were recorded on a Bruker Avance 300 spectrometer at room temperature using perdeuterated solvents as internal standards. Elemental analyses were performed by the Service Chromato-Masse Microanalyse, Université Paris-Saclay (BioCIS), Châtenay-Malabry and by the Service de microanalyse de l'ICSN - CNRS Gif-sur-Yvette, France. Mass spectra were recorded with a MALDI-TOF Microflex LT Bruker.

Luminescence spectra were recorded with a Fluorolog 3 spectrofluorimeter (Horiba Jobin Yvon). Low temperature measurements were realized in an OptistatDN-V Oxford cryostat. The absolute internal quantum yields (Φ) were measured by using the Jobin Yvon integrating sphere. The error of the measured values has been evaluated to 10 %. Emission lifetimes (τ) were recorded with a time-resolved photoluminescence setup consisting of a frequency-tripled regenerative amplified femtosecond Ti:sapphire laser system from Spectra Physics to obtain $\lambda_{\text{ex}} = 267$ nm and a C7700 streak camera from Hamamatsu coupled to an SP2300 imaging Acton spectrograph for the luminescence detection. Data were analyzed by exponential curve fitting using *Origin* software. Spectra in solution were measured in dichloromethane with $c = 10^{-2}$ mol.L⁻¹.

Infrared (IR) spectra from 4000 to 400 cm⁻¹ were recorded with a Bruker Alpha Attenuated Total Reflectance (ATR) spectrometer.

UV-visible absorption spectra were recorded with a Perkin Elmer Lambda 1050 spectrophotometer on dichloromethane solution of the clusters with $c = 10^{-4}$ mol.L⁻¹.

DFT calculations were performed on **C1** and **C2** clusters using the PBE0 functional and the Gaussian 16 suite of programs.⁵⁰ All ground state geometries of **C1** and **C2**, and excited state structure of **C2**, were relaxed and checked to be true minima on the potential energy surface (frequency calculation) using the Def2SVP basis set. For **C1**, we simplified the C₁₂ alkyl chain by a C₆ one, using the ONIOM approach. The C₆ alkyl chain was studied at the PM6 level of theory (low layer), the other parts being studied with the same functional and basis set as for **C2**. Due to the high number of atoms taken into account in the calculation (700), we only studied the ground state properties (IR and absorption). Vibrational contributions to electronic transition responsible for the observed luminescence were taken into account using the Vertical Hessian (VH) approach which takes into account mode-mixing between initial and final states. The lowest normal modes were neglected during the vibronic treatment in order to reach a sufficient progression (> 95 %). This approach gave very good results for such molecular clusters.⁴⁷ All post-treatments were done using the Gaussview, VMS and in-house python codes.⁵¹

Results and Discussions

The five studied phosphine ligands bearing CBP groups (**L1-5**) are presented in Figure 1. The number of CBP groups and their spacing with the PPh₃ moiety, vary within this series in order to evaluate their impact onto the photophysical properties. The previously studied **L1** ligand possesses three CBP groups and a long alkyl chain (C₁₂) as a spacer.⁴⁸ The four other ligands (**L2-4**) present different structures with a lesser number of CBP. **L2** can be seen as the simplest ligand with one CBP group directly grafted onto the phenyl group through an ester group. In **L3** and **L4**, there is an additional spacer between the ester oxygen and the CBP group consisting of a C₂ and C₁₀ alkyl chain, respectively. The **L5** ligand bears two CBPs with a short C₂ spacer such as that of **L3**. Similar to **L1**, the linker is a substituted phenyl group.

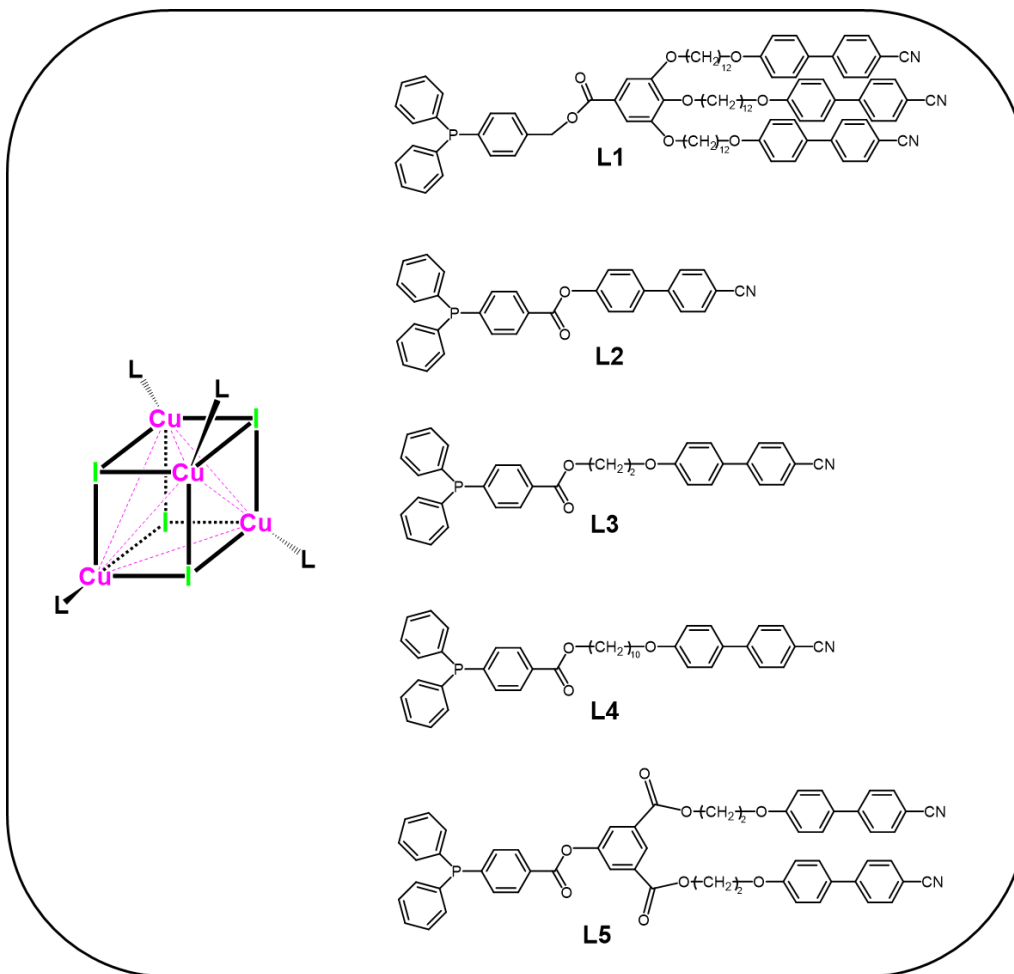


Figure 1. Schematic drawing of the $[\text{Cu}_4\text{I}_4\text{L}_4]$ clusters **C1-5** with the phosphine ligands **L1-5**.

L1 was synthesized according to previous report from 4-(diphenylphosphino)phenylmethanol.⁴⁸ **L2-5** were prepared starting from the carboxylic acid (4-(diphenylphosphino)phenylcarboxylic acid) derivative (experimental details in SI). The corresponding clusters (**C1-5**) were synthesized by reacting CuI with the ligands in dichloromethane at room temperature. All compounds were obtained as white yellowish solids, soluble in most of the common organic solvents. Unfortunately, despite several tries none of these clusters could be crystallized even with the smaller and more rigid **L2** ligand. The formula $[\text{Cu}_4\text{I}_4\text{L}_4]$ (L = ligand) was confirmed by elemental analysis and by ^1H and ^{31}P NMR analyses (details in SI). In particular, the broad ^{31}P peak around -21 ppm is characteristic of the cubane copper iodide clusters.⁵² Differential scanning calorimetry and polarized optical microscopy analyses indicate that **C2-5** are amorphous over the whole temperature range. Therefore these clusters do not present mesomorphic properties in opposite to **C1** which form a Smectic A mesophase upon cooling from 100 °C.⁴⁸

The FTIR spectra were recorded for **C1-5** (Figure S1). To ascertain the vibrational bands assignment, we used the DFT calculations (details in SI and below) performed on **C1** (C_{12} alkyl chain replaced by a shorter C_6 one) and **C2**, within the harmonic approximation since the size of the systems makes impossible anharmonic computations. The simulated IR spectra of **C1** and **C2** are provided in Figure S2 in which a scale factor of 0.96, already used on this type of compound, was applied.^{46,53} The computed vibrational bands of the C=O stretching of the carbonyl group match the experimental ones measured at 1712 and 1732 cm^{-1} for **C1** and **C2**, respectively. Differences experimentally observed between the clusters are also well reproduced by the simulations with a higher energy of the C=O stretching for **C2** than **C1**. This can be explained by the electron acceptor effect of the CBP group to the carbonyl group

that is more pronounced in **C2** having no spacer. The CN stretching is also well localized around 2220 cm^{-1} and is not affected by the modification of the ligand within the clusters series. In the experimental spectra, the band related to long alkyl chain of **C1** and **C4** (C_{12} and C_{10}) stand out around 2900 cm^{-1} . However, these CH_2 vibrations associated to the alkyl chain are wrongly simulated in the 2500-2600 cm^{-1} region for **C1**. This error is due to the PM6 treatment on these moieties during the computation which prevents an accurate vibrational band reproduction. If **C1** was fully treated using the PBE0/Def2SVP approximation, the latter vibrations would be near 2900 cm^{-1} . Computations performed on the single $\text{OH}-(\text{CH}_2)_6-\text{OH}$ molecule using either PM6 and PBE0/Def2SVP fully confirmed the previous statement. Vibrational band observed at 1600 cm^{-1} is attributed to C-C and C-H vibrations from the phenyl rings of the phosphine and that at 815 cm^{-1} to those of the CBP moiety. The doublet at 1494 and 1431 cm^{-1} corresponds to C-H rocking from the other unsubstituted phenyls, in accordance with the vibrational signature of the $[\text{Cu}_4\text{I}_4(\text{PPh}_3)_4]$ cluster (Figure S1).

As shown in Figure 2, **C2** and **C5** solids display a yellow emission at room temperature under UV excitation. The emission of **C3** and **C4** are yellow-green whereas that of **C1** is clearly blueish. When cooled to 77 K, their emission color all becomes more intense and fall into the green with greener emission for **C1**, **C3** and **C4**. When the samples are progressively warmed to room temperature, the initial emissions are recovered. Moderate thermochromic luminescence properties are thus displayed by these clusters with the exception of **C1** which presents a more contrasted temperature-dependent emission color change. The solid-state luminescence spectra of the clusters (**C1-5**) recorded from 293 to 77 K, are reported in Figure 3 and photoluminescence data are gathered in Table 1.

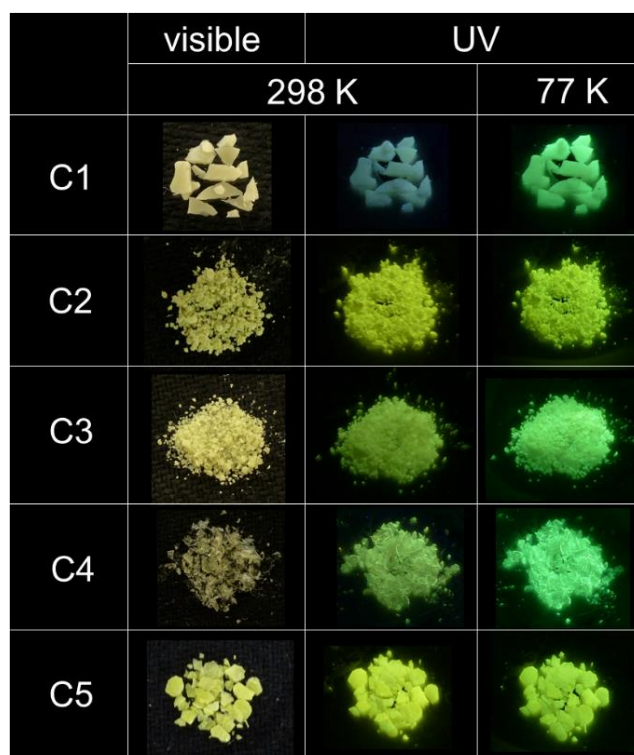
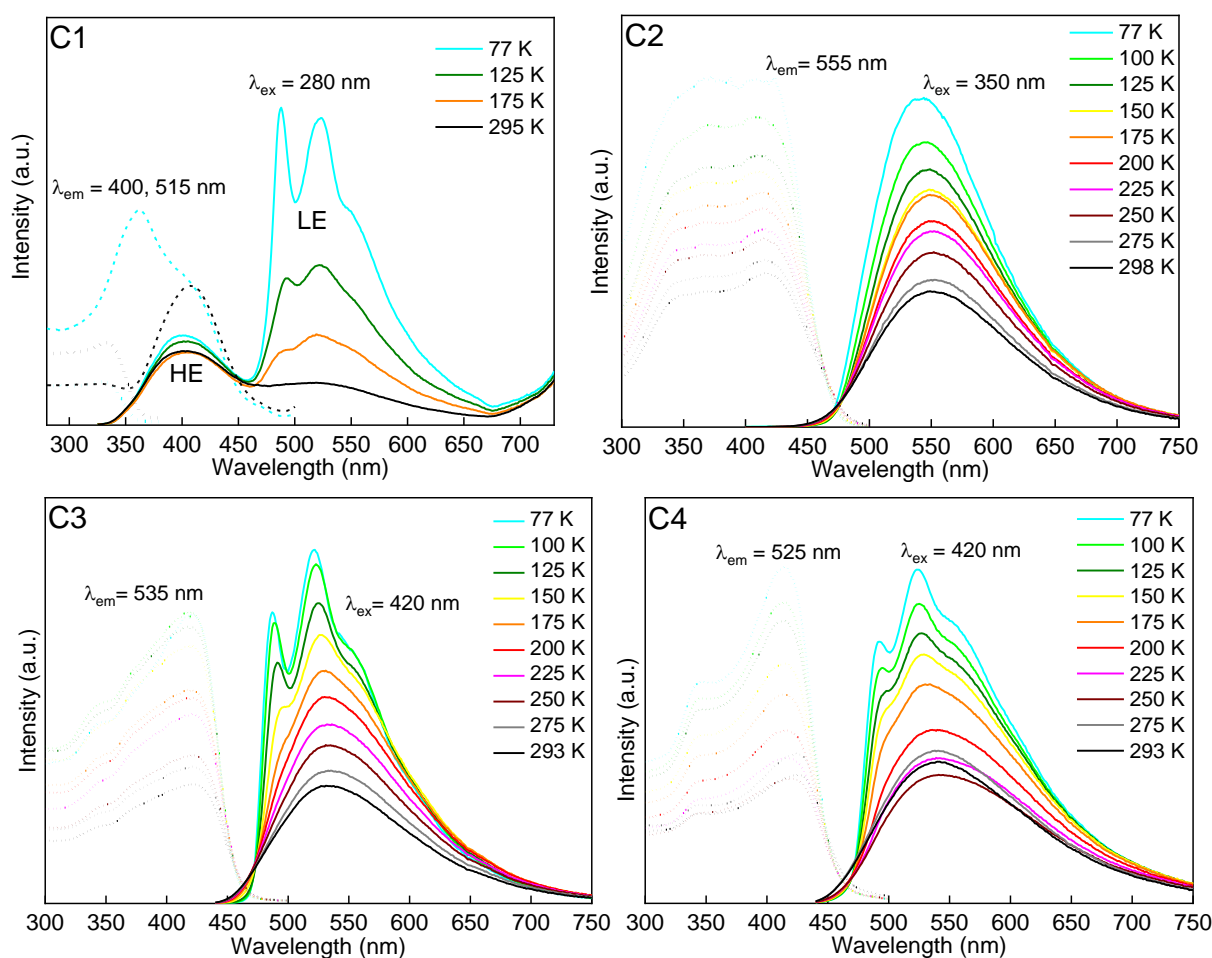


Figure 2. Photos of **C1-5** solids under ambient light and UV irradiation (365 nm lamp) at 298 and 77 K.

At room temperature, **C1** presents two broad unstructured emission bands centered at 404 and 519 nm at $\lambda_{\text{ex}} = 280$ nm, labeled HE (High Energy) and LE (Low Energy), respectively (Figure 3). All the other clusters (**C2-5**) present a similar LE band at 555, 535, 545, 550 nm, respectively. This is in agreement with the yellow emission observed by the naked eyes at 298 K (Figure 2). The HE band is for these

clusters very weak and even undetectable for **C2** in these conditions (Figure S3). Upon excitation at lower energy ($\lambda_{\text{ex}} \sim 400$ nm), the LE band is solely observed for all the clusters (Figure 3 and S4). Excitation profiles are different for the two emission bands. The HE one presents a broad excitation band centered at 300 nm whereas a much wider profile is observed for the LE band ranging from 250 to 450 nm. The quantum yield values corresponding to the LE band are $\Phi = 1, 3.5, 9, 3$ and 14.5 % for **C1-5**, respectively. A value of $\Phi = 9$ % was measured for the HE band of **C1**, that of the other clusters was too weak for such determination. The lifetimes of the LE bands all present decay with similar values in the microsecond scale: $\tau = 1.4, 7.3, 7.2$ and 2.9 μs for **C2-5**, respectively (Figure S5). Shorter values were recorded for the HE bands with monoexponential decay: $\tau = 0.3, 0.4$ and 0.5 μs for **C2, C3** and **C5** (unmeasurable value for **C4**). The LE band of **C1** has a much longer lifetime lying in the millisecond scale: $\tau = 0.3$ ms. In opposite, shorter values were recorded for its HE band: $\tau_1 = 0.1$ and $\tau_2 = 1$ ns. Upon lowering the temperature, the intensity of the LE band increases for all clusters, in accordance to reduction of non-radiative processes. Small blue shift is associated in accordance with the limited emission color change observed for **C2-5**. Nevertheless, an important structuration of the band occurs for **C1, C3** and **C4** with similar profile characterized by two main peaks at ~ 490 and 520 nm (Figure 3). No significant change of the excitation bands is observed over the whole temperature range. **C1** presents however a different excitation profile of the LE band with an additional contribution at around 350 nm. Note that in contrast to **C1** which presents luminescence mechanochromic properties,⁴⁸ **C2-5** are not sensitive to mechanical stimulation. Luminescence vapochromism was not observed for all the clusters.



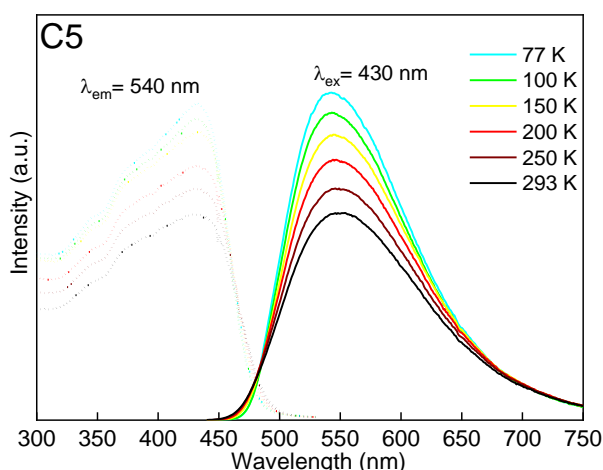


Figure 3. Temperature-dependent solid-state luminescence spectra of **C1-5** from 293 to 77 K, with emission spectra shown as plain lines and excitation spectra as dashed or dotted lines.

The luminescence spectra of the clusters dissolved in dichloromethane are presented in Figure 4a at 298 K. At $\lambda_{\text{ex}} = 280$ nm, all clusters present the two HE and LE emission bands with different relative intensities, excepted **C1** which only displays the HE one. The LE/HE intensity ratio decreases following the order **C2**, **C3**, **C5**, **C4** and **C1**. The HE emission wavelength is similar for **C1** and **C4** at 363 nm and for **C2**, **C3** and **C5** at 356 nm. Different values are found for the LE band at 545, 555, 580 and 590 nm for **C4**, **C3**, **C2** and **C5**, respectively. At $\lambda_{\text{ex}} = 380$ nm (Figure S6), the solely observed LE bands present similar wavelength values as those recorded at $\lambda_{\text{ex}} = 280$ nm. The excitation bands are broader for the LE bands, as expected. Compared with the solid-state, shorter lifetimes values are measured in solution being in the nanosecond range. For the HE bands displaying mono-exponential decay, the values are $\tau = 0.8, 0.3, 0.8$ and 0.3 ns for **C1**, **C3-C5**, respectively (Figure S7). **C2** presents a bi-exponential decay with longer values of $\tau_1 = 0.01$ and $\tau_2 = 0.4$ μs , similar to the solid-state ones. Regarding the LE bands, comparable lifetimes values are found: $\tau = 46, 23, 33$ and 41 ns for **C2-C5**, respectively. UV-vis absorption spectra of the clusters in solution are shown in Figure 4b. The clusters present an intense absorption band centered at 291 nm for **C3** and **C5** and at 296 nm for **C1** and **C4**. This band is redshifted to 275 nm for **C2**. A second weaker band around 355 nm is observed for all clusters excepted for **C1**.

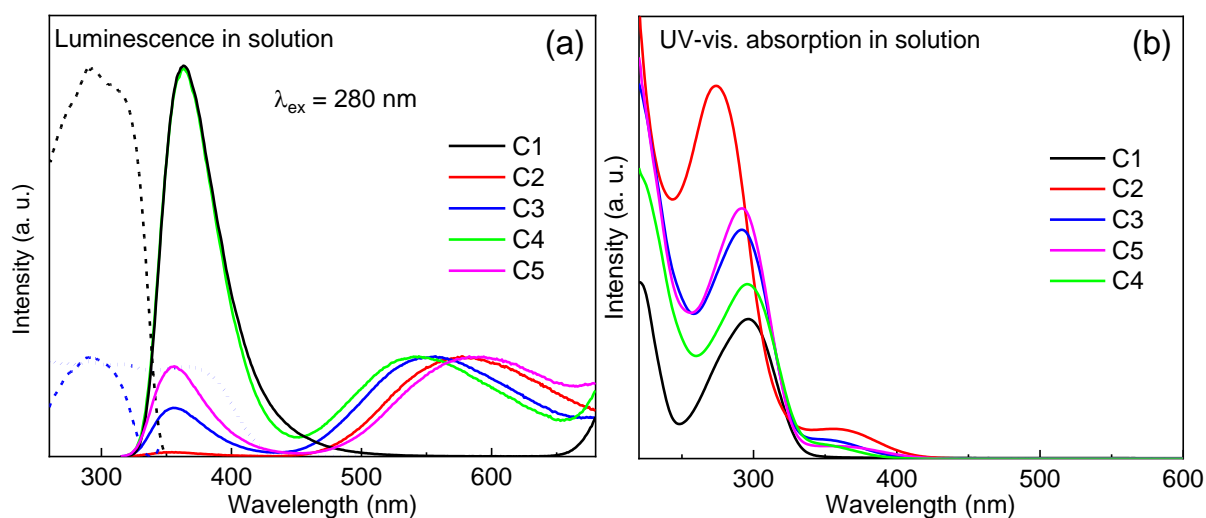


Figure 4. (a) Luminescence spectra of **C1-5** in solution (CH_2Cl_2) at 298 K, with emission spectra shown as plain lines and excitation spectra as dotted lines recorded at maxima of the emission spectra. The LE bands were normalized and for **C1** the intensity of its HE band was adjusted to that of **C4**. (b) UV-visible absorption spectra of **C1-5** in solution (CH_2Cl_2).

Table 1. Photophysical data of **C1-5** at 293 K. Lifetimes recorded at $\lambda_{\text{ex}} = 267$ nm at 298 K. * not measurable due to instrumental artefacts.

	Solid-state			Solution	
	$\lambda_{\text{em}}^{\text{max}}$ (nm) [λ_{ex} (nm)]	τ [λ_{em} (nm)]	QY (%) [λ_{ex} (nm)]	$\lambda_{\text{em}}^{\text{max}}$ (nm) [λ_{ex} (nm)]	τ [λ_{em} (nm)]
C1	404 [280] HE 519 [280] LE	0.1 ns/1 ns [390] HE 0.3 ms [525] LE	9 [280] HE 1 [400] LE	363 [280] HE - LE	0.8 ns [380] HE - LE
C2	- HE 555 [280] LE	0.3 μ s [360] HE 1.4 μ s [540] LE	3.5 [350] LE	355 [280] HE 580 [280] LE	0.01/0.4 μ s [380] HE 2.3/46 ns [580] LE
C3	360 [280] HE 540 [280] LE	0.4 μ s [400] HE 7.3 μ s [540] LE	9 [350] LE	356 [280] HE 555 [280] LE	0.3 ns [380] HE 23 ns [550] LE
C4	358 [280] HE 531 [280] LE	* HE 7.2 μ s [525] LE	3 [350] LE	363 [280] HE 545 [280] LE	0.8 ns [380] HE 33 ns [550] LE
C5	360 [280] HE 550 [280] LE	0.5 μ s [400] HE 2.9 μ s [540] LE	14.5 [350] LE	356 [280] HE 590 [280] LE	0.3 ns [380] HE 41 ns [550] LE

The comparative analysis of the photophysical data of the present clusters, does not lead to straightforward conclusions. Correlation between the spacer length and nature, the number of CBP group, and the photoluminescence properties is far from direct. The origin of the emission bands is also difficult to assign since the photophysical properties of **C1-5** present significant differences compared with those of the more classical cubane clusters. Indeed, the [Cu₄I₄L₄] clusters with PPh₂R ligands commonly displayed a broad unstructured emission band at room temperature (LE) whose intensity decreases upon lowering the temperature in detriment to a higher energy band (HE). The variation in temperature of the relative intensities of these two bands is at the origin of the luminescence thermochromism depicted by this family of compounds. From previous studies, the LE band is a transition of mixed XMCT and MM character (X = I and M = Cu).⁴⁵ The corresponding triplet excited state is commonly labelled ³CC (Cluster Centered), and involved a Cu-Cu bonding vacant orbital (LUMO+24 for [Cu₄I₄(PPh₃)₄]). A significant Cu-Cu shortening thus occurs for this triplet state compared with the fundamental one. The nature of the HE band is different and implies the phenyl groups of the phosphine ligands and the corresponding transition is of ³(X,M)LCT character. The thermal equilibrium between the two corresponding excited triplet states leads to the opposite intensity variation of these two emission bands. At first sight, the broad emission band observed for **C1-5** at room temperature can be attributed to the LE band classically observed for the cubane [Cu₄I₄L₄] clusters. The emission maxima are indeed similar to that reported for [Cu₄I₄(PPh₃)₄] of 545 nm, with an emission lifetime value in the microsecond range ($\tau = 4.3 \mu\text{s}$).⁴⁵ However, the well resolved structuration of the LE band is untypical for these clusters. Such structuration has been already observed for the band involving the ligand orbitals but never for the ³CC one. This suggests that the origin of the LE emission band of **C1-5** is probably different from the ³CC one. Regarding the HE band of **C1-5**, the ligand orbitals may imply π^* phenyl orbitals of the phosphine moiety and/or of the CBP units. The nature of the HE and LE emission bands of **C1-5** thus appears significantly different from those of the [Cu₄I₄L₄] cubane clusters, that motivated density functional theory (DFT) calculations to elucidate their origin.

Due to the large size of the studied systems, DFT calculations were only performed on **C1** and **C2** clusters. Comparisons of these two clusters could indeed permit to study the effect of both the spacer and the number of CBP groups. The alkyl chain was reduced from C₁₂ to C₆ for **C1** to lower calculations duration while preserving the effect of a long spacer. The geometry at the ground state (S₀) was optimized in (C₁) and (C₂) symmetry for **C1** and **C2**, respectively, and the calculated molecular structures are presented in Figure 5. Regarding the more symmetrical **C2** cluster, the Cu-I bond lengths between 2.700 and 2.734 Å and the Cu-P ones of 2.343 and 2.347 Å, are in accordance with those

reported for cubane copper iodide clusters coordinated by phosphine ligands.^{45,52} The Cu-Cu distances of the Cu₄ tetrahedron of **C2** lie in the 2.733-2.776 Å range. These distances are shorter than those reported in the literature for such phosphine-based clusters with a mean value of 3.1 Å.⁵⁴ This underestimation is attributed to the Def2SVP basis set used. The calculated Cu-Cu, Cu-I and Cu-P distances of **C1** are very close to those of **C2** (Figure 5).

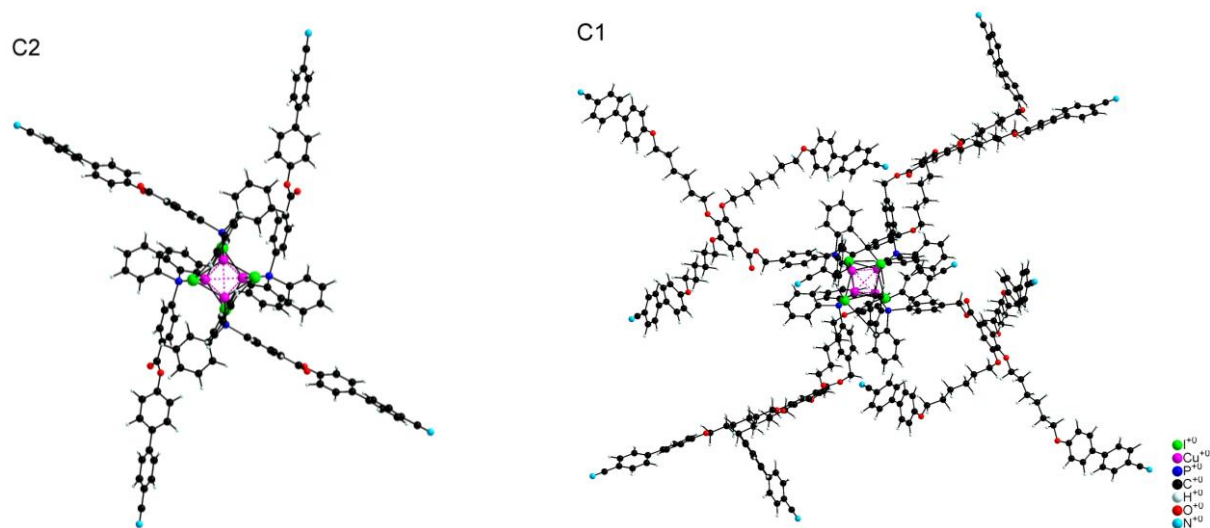
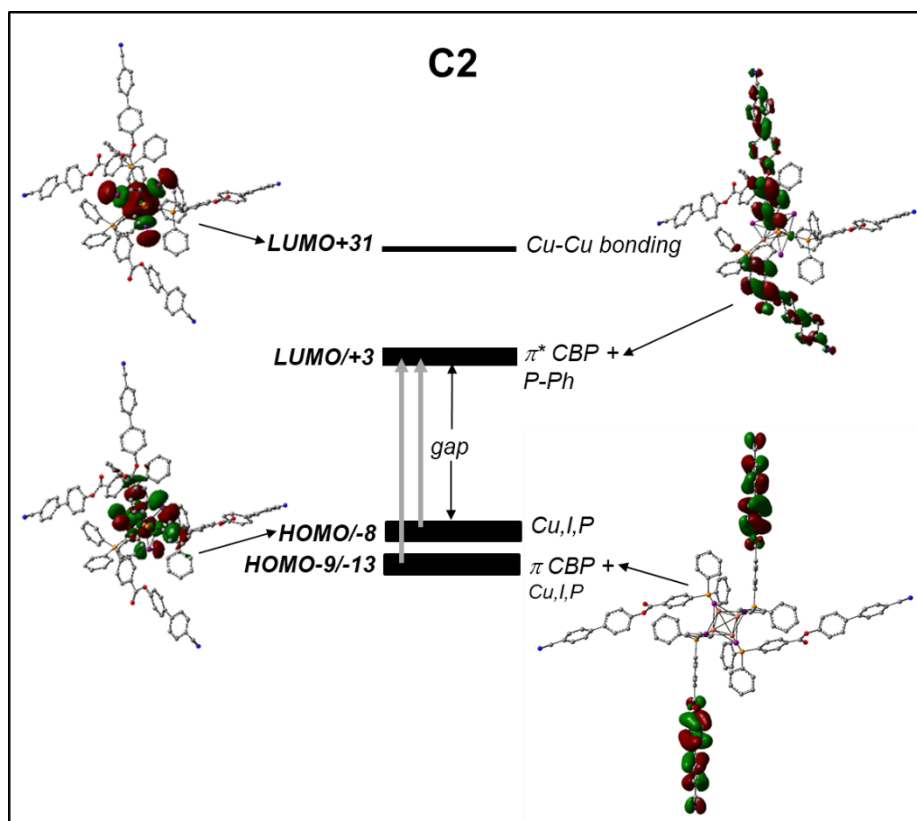


Figure 5. Optimized molecular structure (S_0) of **C2** in (C_2) symmetry (Cu-Cu: 2.733-2.776; Cu-I: 2.700-2.734; Cu-P: 2.343-2.347 Å) and of **C1** with a shorter alkyl chain spacer C_6 in (C_1) symmetry (Cu-Cu: 2.722-2.801; Cu-I: 2.707-2.741; Cu-P: 2.345-2.349 Å).

The simplified orbital diagrams for **C2** and **C1** at the ground state (S_0) are presented in Figure 6 along with representation of selected orbitals. For both clusters, the highest occupied molecular orbitals (HOMOs) are mainly located on the inorganic cluster core with Cu, I and P contributions. In contrast, the lowest unoccupied molecular orbitals (LUMOs) are based on the ligand with a dominant CBP character with, for **C2**, an additional contribution of the ester substituted phenyl group bond to the P atom (P-Ph). The latter result agrees with the strong electron acceptor character of the CN group. The computed HOMO-LUMO gaps are ~ 6.60 eV and 3.55 eV, for **C1** and **C2**, respectively. This large difference between both values is probably due to the QM/MM approach used for **C1** which might cause a larger bandgap. The computed gap value of **C2** is however lower than the computed ones in previous reports^{45,46,52} and is attributed to the CN group which stabilizes the LUMO. Above the block of CBP-based LUMOs of **C1**, are vacant orbitals involving the substituted phenyl group (Ph-O3). The classical Cu-Cu bonding vacant orbital of the cubane clusters implied in the LE emission, generally lies just above the ligand-based orbitals. In the case of **C2**, this bonding orbital is found at very high energy (~ 5 eV from the HOMO) and is the LUMO+31 (shown in Figure 6). It might stand at even higher energy for **C1**. TDDFT computations were performed to assign the observed absorption bands. Transitions of two different natures were computed for **C2** (Table S1). At 294 and 297 nm, the corresponding transitions is HOMO-9/HOMO-13 \rightarrow LUMO/LUMO+3 (π CBP + Cu,I $\rightarrow \pi^*$ CBP + P-Ph). These transitions can correspond to the high energy absorption bands observed experimentally at 275-296 nm (Figure 4), and can thus be assigned to CBP-based transitions mainly. The other transitions computed at 334, 406 and 419 nm are HOMO-LUMO transitions (HOMO/HOMO-5 \rightarrow LUMO/LUMO+3; Cu,I,P $\rightarrow \pi^*$ CBP + P-Ph) and correspond to the experimental broad absorption band centered at 355 nm. This charge transfer transition thus labelled $^1(X+M)LCT$, is common for copper iodide complexes. For **C1**, the computed transitions of highest oscillator strengths (386 and 400 nm) are from the HOMO/HOMO-2 to

the LUMO/LUMO+2 implying a charge transfer from the cluster core to the CBP group. With a long alkyl chain acting as a spacer, one may explain the transition as a charge transfer between two independent moieties. This result was not considered further because such charge transfer is hardly possible due to the large distance separating those moieties and the very low oscillator strengths associated. Much more plausible $^1(X+M)LCT$ charge transfer transitions are HOMO/HOMO-9 \rightarrow LUMO+10 implying in this case the substituted phenyl group (Ph-O3) closer to the cluster core.



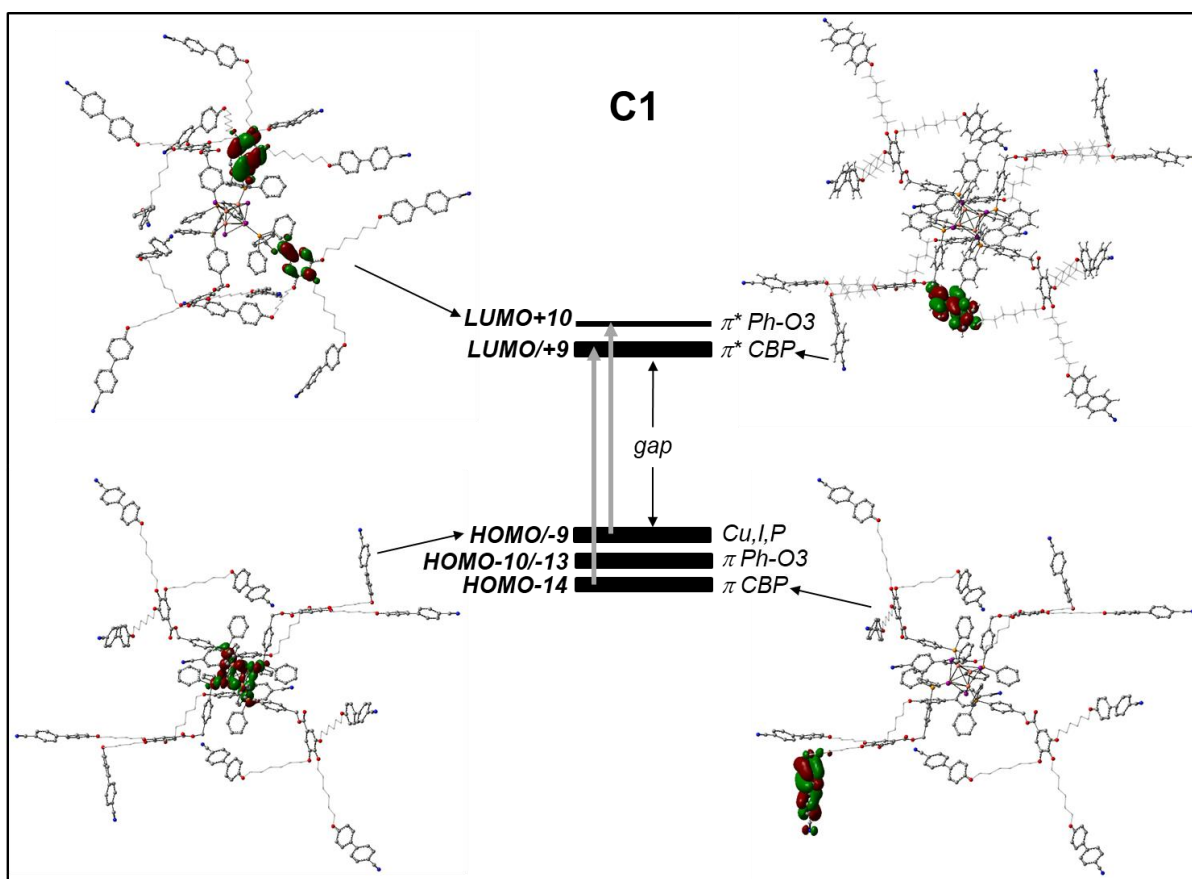


Figure 6. Simplified orbital diagram of **C2** and **C1** at the ground state (S_0). Orbital compositions are indicated along with representations of the orbitals (iodide in purple, copper and phosphorus in orange, oxygen in red, nitrogen in blue and carbon in grey), hydrogen atoms are omitted for clarity.

Cluster **C1** is too large and prevents the study of its excited state with quantum calculations. On the contrary, although **C2** possesses more than 200 atoms, we were able to converge a triplet excited state structure and confirm its stability. The geometry of the structure of this excited state is similar to that of the fundamental state with a barely modified $[Cu_4I_4]$ cluster core (Figure S8). The calculated spin density shows that the free electrons are indeed mostly localized on the PPh_3 moiety with some contribution of the iodide atoms (Figure S9). This state thus differs from the classical 3CC excited one since here a strong implication of the ligand is observed. The corresponding transition can thus be assigned to ${}^3(X+M)LCT$. The luminescence spectrum was computed using the VH ansatz, already used in previous communications.⁴⁶ As shown in Figure 7, the recorded solid-state emission band of **C2** centered at 555 nm is very well reproduced by the simulation, supporting the previous ${}^3(X+M)LCT$ assignment.

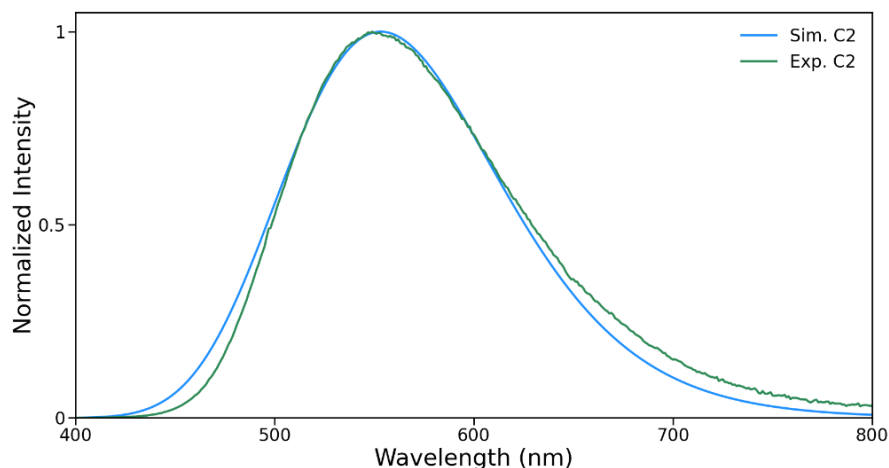


Figure 7. Simulated emission spectra of the triplet state and experimental solid-state emission spectra of **C2**.

Based on the DFT results, the LE emission band of **C1-5** clusters can be assigned to the charge-transfer transition ${}^3(\text{X+M})\text{LCT}$ and is thus different from the classical ${}^3\text{CC}$ state of other cubane clusters. This can be easily explained by the high energy of the Cu-Cu bonding vacant orbital being thus inaccessible. It can be additionally related to the low energy of the ligand-based vacant orbitals due to the electron acceptor character of the CN groups. This ${}^3(\text{X+M})\text{LCT}$ emission is indeed of lower energy compared with that of the classical clusters such that of $[\text{Cu}_4\text{I}_4(\text{PPh}_3)_4]$ centered at 420 nm.⁴⁵ The lifetime values in the microsecond range are however similar in both cases. The structuration observed of this ${}^3(\text{X+M})\text{LCT}$ emission at low temperature can thus be attributed to vibronic effect in accordance to its ligand character and similar excitation signature of the components. The lack of such structuration for **C2** and **C5** is difficult to rationalize at this stage, and in particular based on the rigidity of the ligand which is not superior for **L1**, **L3-4** compared with **L2** and **L5** without long alkyl chain. Vibronic structuration probably occurs at lower temperatures for **C2** and **C5**.

Regarding the HE emission band, its origin can be attributed to an intra-ligand (IL) $\pi\text{-}\pi^*$ transition centered on the CBP group, in analogy with previous reports on CBP derivatives.⁵⁵⁻⁵⁹ The monomer emission reported around 370 nm can be shifted to lower energy for excimers. The HE band of **C1** at $\lambda_{\text{max}} = 363$ nm in solution can be thus attributed to monomers whereas excimers are formed in solid-state with $\lambda_{\text{max}} = 404$ nm. This is in accordance with the nanosecond time scale of the lifetimes measured in solution, and previous reports.⁵⁵⁻⁵⁹ Corresponding CBP IL absorption transitions around 300 nm were confirmed by the calculations. The redshift of this absorption band for **C2** ($\lambda_{\text{max}} = 275$ nm) compared with that of the others clusters, can be due to electronic effect of the PPh_3 moiety onto the CBP, stronger in that case without any spacer. This may also explain the different lifetime of the HE band (μs) in solution of **C2** compared with that of the other clusters values (ns).

Upon lowering the temperature, the concomitant increase of the intensity of the two HE and LE emission bands of **C1** is different from the thermochromism classically observed based on thermal equilibrium between the two emissive states. This unclassical feature is in agreement with the different origin of the emissions. Among the studied clusters, **C1** presents the more intense HE band that can be explained by the larger number of CBP groups born by its ligand. However, the HE band intensity of **C5** having two CBP groups per ligand is not higher compared with that of **C4** having only one CBP group. This observation indicates a possible energy transfer between the two emissive centers. Indeed, occurrence of such transfer is supported by the spectral overlap between the HE emission band and the LE absorption band. The excitation profile of the LE bands in solid-state is also clearly different from that

of classical clusters with a maximum around 400 nm corresponding to this spectral overlap area. A FRET (Förster Resonance Energy Transfer) mechanism between the CBP group (acting as donor) and the cluster (acting as acceptor) is indeed possible based on the distances separating these two emitters which are in the relevant 1-10 nm range.⁶⁰ The much higher intensity of the HE bands of all clusters in solution compared with those in solid-state, can be explained by the transfer efficiency being reduced in solution due to molecular motion and decrease of the distance between emitters.⁶¹ Full transfer in solid-state leads to an almost extinguished HE band for the clusters. The case of **C1** is different for which the transfer is only partial resulting in remaining HE emission and leading to a dual emissive system. The particularity of **C1** such as the uncommon long lifetime (ms) of its LE band can find its origin in its liquid crystalline properties with a specific organization of the CBP groups and excimers formation, known to impact the photophysical properties. The relative orientation between the donor and acceptor is also known to impact the energy transfer efficiency. The strong distance-dependency of the FRET process is also illustrated along this cluster series. The predominance of the HE band for **C1** and **C4** compared with its near extinction for **C2** is consistent with the long spacers (**C10** and **C12**) for the former, and the lack of it for the latter. **C3** and **C5** having short spacer represent intermediate cases. Lifetimes values are shorter in the solution compared with the solid-state as expected, but conclusions regarding the precise nature of the energy transfer process are difficult to be drawn. The CBP-[Cu₄I₄] clusters are indeed more complexes than two fully independent emitters usually at play in FRET studies.

Conclusions.

The present comparative study of five copper iodide clusters functionalized by different CBP-based phosphine ligands demonstrates the impact of the emissive properties of the ligands onto the photophysical properties of the cluster entirety. Compared with classical [Cu₄I₄L₄] copper iodide clusters, the origin of the emission bands is completely different. The CBP moiety of electron acceptor character significantly lowers in energy the vacant orbitals and consequently the (X,M)LCT emission band. The cluster core emission is therefore not accessible anymore. The intrinsic emission of the CBP moiety brings an additional emission band at higher energy. This dual emissive system thus differs from the classical clusters by having two different emissive centers which are interacting through energy transfer.

These CBP-[Cu₄I₄] photoactive systems show that the design of original ligands can effectively enrich the photophysical properties of these family of copper iodide complexes. By using ligands with suitable emissive states, a neat control of the photoluminescence properties can be even envisioned. The study of original photoactive ligands indeed opens new perspectives towards multifunctional materials. Such investigations are currently under progress in our group.

Acknowledgments.

R. U.-M. thanks the DGA and the 'Région Pays de la Loire' for her Ph.D. fellowship. CCIPL (Centre de Calculs Intensifs des Pays de Loire) is acknowledged for computational resources.

Supporting Information. FTIR spectra, emission decay curves and additional luminescence spectra and DFT calculations data. This information is available free of charge at <http://pubs.acs.org>.

References.

- (1) Wenger, O. S. Photoactive Complexes with Earth-Abundant Metals. *J. Am. Chem. Soc.* **2018**, *140* (42), 13522–13533. <https://doi.org/10.1021/jacs.8b08822>.

- (2) Yu, T.-L.; Guo, Y.-M.; Wu, G.-X.; Yang, X.-F.; Xue, M.; Fu, Y.-L.; Wang, M.-S. Recent Progress of D10 Iodoargentate(I)/Iodocuprate(I) Hybrids: Structural Diversity, Directed Synthesis, and Photochromic/Thermochromic Properties. *Coord. Chem. Rev.* **2019**, *397*, 91–111. <https://doi.org/10.1016/j.ccr.2019.06.006>.
- (3) Hamze, R.; Peltier, J. L.; Sylvinson, D.; Jung, M.; Cardenas, J.; Haiges, R.; Soleilhavoup, M.; Jazzar, R.; Djurovich, P. I.; Bertrand, G.; Thompson, M. E. Eliminating Nonradiative Decay in Cu(I) Emitters: >99% Quantum Efficiency and Microsecond Lifetime. *Science* **2019**, *363* (6427), 601–606. <https://doi.org/10.1126/science.aav2865>.
- (4) Olaru, M.; Rychagova, E.; Ketkov, S.; Shynkarenko, Y.; Yakunin, S.; Kovalenko, M. V.; Yablonskiy, A.; Andreev, B.; Kleemiss, F.; Beckmann, J.; Vogt, M. A Small Cationic Organo–Copper Cluster as Thermally Robust Highly Photo- and Electroluminescent Material. *J. Am. Chem. Soc.* **2020**, *142* (1), 373–381. <https://doi.org/10.1021/jacs.9b10829>.
- (5) Baghdasaryan, A.; Bürgi, T. Copper Nanoclusters: Designed Synthesis, Structural Diversity, and Multiplatform Applications. *Nanoscale* **2021**, *13* (13), 6283–6340. <https://doi.org/10.1039/D0NR08489A>.
- (6) Schlachter, A.; Tanner, K.; Harvey, P. D. Copper Halide-Chalcogenoether and -Chalcogenone Networks: Chain and Cluster Motifs, Polymer Dimensionality and Photophysical Properties. *Coord. Chem. Rev.* **2021**, *448*, 214176. <https://doi.org/10.1016/j.ccr.2021.214176>.
- (7) Yao, J.-S.; Wang, J.-J.; Yang, J.-N.; Yao, H.-B. Modulation of Metal Halide Structural Units for Light Emission. *Acc. Chem. Res.* **2021**, *54* (2), 441–451. <https://doi.org/10.1021/acs.accounts.0c00707>.
- (8) Troyano, J.; Zamora, F.; Delgado, S. Copper(I)–Iodide Cluster Structures as Functional and Processable Platform Materials. *Chem. Soc. Rev.* **2021**, *50* (7), 4606–4628. <https://doi.org/10.1039/D0CS01470B>.
- (9) Liu, G.-N.; Xu, R.-D.; Zhao, R.-Y.; Sun, Y.; Bo, Q.-B.; Duan, Z.-Y.; Li, Y.-H.; Wang, Y.-Y.; Wu, Q.; Li, C. Hybrid Copper Iodide Cluster-Based Pellet Sensor for Highly Selective Optical Detection of o-Nitrophenol and Tetracycline Hydrochloride in Aqueous Solution. *ACS Sustainable Chem. Eng.* **2019**, *7* (23), 18863–18873. <https://doi.org/10.1021/acssuschemeng.9b03963>.
- (10) Fang, Y.; Soj dak, C. A.; Dey, G.; Teat, S. J.; Li, M.; Cotlet, M.; Zhu, K.; Liu, W.; Wang, L.; ÓCarroll, D. M.; Li, J. Highly Efficient and Very Robust Blue-Excitable Yellow Phosphors Built on Multiple-Stranded One-Dimensional Inorganic–Organic Hybrid Chains. *Chem. Sci.* **2019**, *10* (20), 5363–5372. <https://doi.org/10.1039/C9SC00970A>.
- (11) Kitagawa, H.; Ohtsu, H.; Kawano, M. Kinetic Assembly of a Thermally Stable Porous Coordination Network Based on Labile CuI Units and the Visualization of I₂ Sorption. *Angew. Chem. Int. Ed.* **2013**, *52* (47), 12395–12399. <https://doi.org/10.1002/anie.201306776>.
- (12) Peng, R.; Li, M.; Li, D. Copper(I) Halides: A Versatile Family in Coordination Chemistry and Crystal Engineering. *Coord. Chem. Rev.* **2010**, *254* (1–2), 1–18. <https://doi.org/10.1016/j.ccr.2009.10.003>.
- (13) Yam, V. W.-W.; Au, V. K.-M.; Leung, S. Y.-L. Light-Emitting Self-Assembled Materials Based on d⁸ and d¹⁰ Transition Metal Complexes. *Chem. Rev.* **2015**, *115* (15), 7589–7728. <https://doi.org/10.1021/acs.chemrev.5b00074>.
- (14) Kobayashi, A.; Kato, M. Stimuli-Responsive Luminescent Copper(I) Complexes for Intelligent Emissive Devices. *Chem. Lett.* **2017**, *46* (2), 154–162. <https://doi.org/10.1246/cl.160794>.
- (15) Cariati, E.; Lucenti, E.; Botta, C.; Giovanella, U.; Marinotto, D.; Righetto, S. Cu(I) Hybrid Inorganic–Organic Materials with Intriguing Stimuli Responsive and Optoelectronic Properties. *Coord. Chem. Rev.* **2016**, *306*, 566–614. <https://doi.org/10.1016/j.ccr.2015.03.004>.
- (16) Wallesch, M.; Volz, D.; Zink, D. M.; Schepers, U.; Nieger, M.; Baumann, T.; Bräse, S. Bright Coppertunities: Multinuclear CuI Complexes with NP Ligands and Their Applications. *Chem. Eur. J.* **2014**, *20*, 6578–6590. <https://doi.org/10.1002/chem.201402060>.
- (17) Wang, J.-H.; Li, M.; Li, D. A Dynamic, Luminescent and Entangled MOF as a Qualitative Sensor for Volatile Organic Solvents and a Quantitative Monitor for Acetonitrile Vapour. *Chem. Sci.* **2013**, *4* (4), 1793. <https://doi.org/10.1039/c3sc00016h>.

- (18) Yu, Y.; Zhang, X.-M.; Ma, J.-P.; Liu, Q.-K.; Wang, P.; Dong, Y.-B. Cu(I)-MOF: Naked-Eye Colorimetric Sensor for Humidity and Formaldehyde in Single-Crystal-to-Single-Crystal Fashion. *Chem. Commun.* **2014**, *50* (12), 1444–1446. <https://doi.org/10.1039/C3CC47723A>.
- (19) Conesa-Egea, J.; Zamora, F.; Amo-Ochoa, P. Perspectives of the Smart Cu-Iodine Coordination Polymers: A Portage to the World of New Nanomaterials and Composites. *Coordination Chemistry Reviews* **2019**, *381*, 65–78. <https://doi.org/10.1016/j.ccr.2018.11.008>.
- (20) Shi, D.; Zheng, R.; Sun, M.-J.; Cao, X.; Sun, C.-X.; Cui, C.-J.; Liu, C.-S.; Zhao, J.; Du, M. Semiconductive Copper(I)-Organic Frameworks for Efficient Light-Driven Hydrogen Generation Without Additional Photosensitizers and Cocatalysts. *Angew. Chem. Int. Ed.* **2017**, *56* (46), 14637–14641. <https://doi.org/10.1002/anie.201709869>.
- (21) Zink, D. M.; Volz, D.; Baumann, T.; Mydlak, M.; Flu, H.; Friedrichs, J.; Nieger, M.; Bras, S. Heteroleptic, Dinuclear Copper(I) Complexes for Application in Organic Light-Emitting Diodes. *Chem. Mater.* **2013**, *25*, 4471–4486. <https://doi.org/10.1021/cm4018375>.
- (22) Liu, Z.; Qiu, J.; Wei, F.; Wang, J.; Liu, X.; Helander, M. G.; Rodney, S.; Wang, Z.; Bian, Z.; Lu, Z.; Thompson, M. E.; Huang, C. Simple and High Efficiency Phosphorescence Organic Light-Emitting Diodes with Codeposited Copper(I) Emitter. *Chem. Mater.* **2014**, *26*, 2368–2373. <https://doi.org/10.1021/cm5006086>.
- (23) You, Z.; Li, H.; Zhang, L.; Yu, B.; Zhang, J.; Wu, X. A Host Material for Deep-Blue Electrophosphorescence Based on a Cuprous Metal–Organic Framework. *J. Phys. Chem. C* **2017**, *121* (41), 23072–23079. <https://doi.org/10.1021/acs.jpcc.7b07627>.
- (24) Zhu, K.; Cheng, Z.; Rangan, S.; Cotlet, M.; Du, J.; Kasaei, L.; Teat, S. J.; Liu, W.; Chen, Y.; Feldman, L. C.; O’Carroll, D. M.; Li, J. A New Type of Hybrid Copper Iodide as Nontoxic and Ultrastable LED Emissive Layer Material. *ACS Energy Lett.* **2021**, *6* (7), 2565–2574. <https://doi.org/10.1021/acsenerylett.1c00993>.
- (25) Liu, Y.; Yiu, S.-C.; Ho, C.-L.; Wong, W.-Y. Recent Advances in Copper Complexes for Electrical/Light Energy Conversion. *Coord. Chem. Rev.* **2018**, *375*, 514–557. <https://doi.org/10.1016/j.ccr.2018.05.010>.
- (26) Hardt, H. D.; Pierre, A. Fluorescence Thermochromism of Pyridine Copper Iodides and Copper Iodide. *Z. Anorg. Allg. Chem.* **1973**, *402* (1), 107–112. <https://doi.org/10.1002/zaac.19734020113>.
- (27) Radjaipour, M.; Oelkrug, D. Kinetik der Lumineszenz-Thermochromie und Zuordnung der Tieftemperaturmission von Pyridino-Kupfer(I)-jodid. *Ber. Bunsen-Ges. Phys. Chem.* **1978**, *82* (2), 159–163. <https://doi.org/10.1002/bbpc.197800004>.
- (28) Ford, P. C.; Cariati, E.; Bourassa, J. Photoluminescence Properties of Multinuclear Copper(I) Compounds. *Chem. Rev.* **1999**, *99* (12), 3625–3648. <https://doi.org/10.1021/cr960109i>.
- (29) Kim, T. H.; Shin, Y. W.; Jung, J. H.; Kim, J. S.; Kim, J. Crystal-to-Crystal Transformation between Three CuI Coordination Polymers and Structural Evidence for Luminescence Thermochromism. *Angew. Chem. Int. Ed.* **2008**, *47* (4), 685–688. <https://doi.org/10.1002/anie.200704349>.
- (30) Fu, Z.; Lin, J.; Wang, L.; Li, C.; Yan, W.; Wu, T. Cuprous Iodide Pseudopolymorphs Based on Imidazole Ligand and Their Luminescence Thermochromism. *Crystal Growth & Design* **2016**, *16* (4), 2322–2327. <https://doi.org/10.1021/acs.cgd.6b00114>.
- (31) Zhan, S.-Z.; Li, M.; Ng, S. W.; Li, D. Luminescent Metal-Organic Frameworks (MOFs) as a Chemopalette: Tuning the Thermochromic Behavior of Dual-Emissive Phosphorescence by Adjusting the Supramolecular Microenvironments. *Chem. Eur. J.* **2013**, *19* (31), 10217–10225. <https://doi.org/10.1002/chem.201204632>.
- (32) Perruchas, S. Molecular Copper Iodide Clusters: A Distinguishing Family of Mechanochromic Luminescent Compounds. *Dalton Transactions* **2021**, *50* (35), 12031–12044. <https://doi.org/10.1039/D1DT01827B>.
- (33) Zhao, C.-W.; Ma, J.-P.; Liu, Q.-K.; Wang, X.-R.; Liu, Y.; Yang, J.; Yang, J.-S.; Dong, Y.-B. An in Situ Self-Assembled Cu₄I₄-MOF-Based Mixed Matrix Membrane: A Highly Sensitive and Selective Naked-Eye Sensor for Gaseous HCl. *Chem. Commun.* **2016**, *52* (30), 5238–5241. <https://doi.org/10.1039/C6CC00189K>.

- (34) Cho, S.; Jeon, Y.; Lee, S.; Kim, J.; Kim, T. H. Reversible Transformation between Cubane and Stairstep Cu_4I_4 Clusters Using Heat or Solvent Vapor. *Chem. Eur. J.* **2015**, *21* (4), 1439–1443. <https://doi.org/10.1002/chem.201405800>.
- (35) Park, H.; Kwon, E.; Chiang, H.; Im, H.; Lee, K. Y.; Kim, J.; Kim, T. H. Reversible Crystal Transformations and Luminescence Vapochromism by Fast Guest Exchange in Cu(I) Coordination Polymers. *Inorg. Chem.* **2017**, *56* (14), 8287–8294. <https://doi.org/10.1021/acs.inorgchem.7b00951>.
- (36) Killarney, J. P.; McKinnon, M.; Murphy, C.; Henline, K. M.; Wang, C.; Pike, R. D.; Patterson, H. H. Amine- and Sulfide-Sensing Copper(I) Iodide Films. *Inorg. Chem. Com.* **2014**, *40*, 18–21. <https://doi.org/10.1016/j.inoche.2013.11.022>.
- (37) Tran, D.; Bourassa, J. L.; Ford, P. C. Pressure-Induced Luminescence Rigidochromism in the Photophysics of the Cuprous Iodide Cluster $Cu_4I_4py_4$. *Inorg. Chem.* **1997**, *36* (3), 439–442. <https://doi.org/10.1021/ic960959g>.
- (38) Vogler, Arnd.; Kunkely, Horst. Photoluminescence of Tetrameric Copper(I) Iodide Complexes Solutions. *J. Am. Chem. Soc.* **1986**, *108* (23), 7211–7212. <https://doi.org/10.1021/ja00283a012>.
- (39) Roppolo, I.; Celasco, E.; Sangermano, M.; Garcia, A.; Gacoin, T.; Boilot, J.-P.; Perruchas, S. Luminescence Variation by Rigidity Control of Acrylic Composite Materials. *J. Mater. Chem. C* **2013**, *1* (36), 5725. <https://doi.org/10.1039/c3tc30407h>.
- (40) Chen, C.; Li, R.-H.; Zhu, B.-S.; Wang, K.-H.; Yao, J.-S.; Yin, Y.-C.; Yao, M.-M.; Yao, H.-B.; Yu, S.-H. Highly Luminescent Inks: Aggregation-Induced Emission of Copper-Iodine Hybrid Clusters. *Angew. Chem. Int. Ed.* **2018**, *57* (24), 7106–7110. <https://doi.org/10.1002/anie.201802932>.
- (41) Fang, Y.; Liu, W.; Teat, S. J.; Dey, G.; Shen, Z.; An, L.; Yu, D.; Wang, L.; O'Carroll, D. M.; Li, J. A Systematic Approach to Achieving High Performance Hybrid Lighting Phosphors with Excellent Thermal- and Photostability. *Adv. Funct. Mater.* **2017**, *27* (3), 1603444. <https://doi.org/10.1002/adfm.201603444>.
- (42) Xie, M.; Han, C.; Zhang, J.; Xie, G.; Xu, H. White Electroluminescent Phosphine-Chelated Copper Iodide Nanoclusters. *Chem. Mater.* **2017**, *29* (16), 6606–6610. <https://doi.org/10.1021/acs.chemmater.7b01443>.
- (43) Xie, M.; Han, C.; Liang, Q.; Zhang, J.; Xie, G.; Xu, H. Highly Efficient Sky Blue Electroluminescence from Ligand-Activated Copper Iodide Clusters: Overcoming the Limitations of Cluster Light-Emitting Diodes. *Sci. Adv.* **2019**, *5* (6), eaav9857. <https://doi.org/10.1126/sciadv.aav9857>.
- (44) Churchill, M. R.; Kalra, K. L. Molecules with an M_4X_4 Core. I. Crystal and Molecular Structure of Tetrameric Triphenylphosphinecopper(I) Chloride, a “Cubane-Like” Molecule, Including the Location and Refinement of All Hydrogen Atoms. *Inorg. Chem.* **1974**, *13* (5), 1065–1071. <https://doi.org/10.1021/ic50135a011>.
- (45) Perruchas, S.; Tard, C.; Le Goff, X. F.; Fargues, A.; Garcia, A.; Kahlal, S.; Saillard, J.-Y.; Gacoin, T.; Boilot, J.-P. Thermochromic Luminescence of Copper Iodide Clusters: The Case of Phosphine Ligands. *Inorg. Chem.* **2011**, *50* (21), 10682–10692. <https://doi.org/10.1021/ic201128a>.
- (46) Utrera-Melero, R.; Huitorel, B.; Cordier, M.; Mevellec, J.-Y.; Massuyeau, F.; Latouche, C.; Martineau-Corcus, C.; Perruchas, S. Combining Theory and Experiment to Get Insight into the Amorphous Phase of Luminescent Mechanochromic Copper Iodide Clusters. *Inorg. Chem.* **2020**, *59* (18), 13607–13620. <https://doi.org/10.1021/acs.inorgchem.0c01967>.
- (47) Utrera-Melero, R.; Huitorel, B.; Cordier, M.; Massuyeau, F.; Mevellec, J.-Y.; Stephant, N.; Deniard, P.; Latouche, C.; Martineau-Corcus, C.; Perruchas, S. Mechanically Responsive Luminescent Films Based on Copper Iodide Clusters. *J. Mater. Chem. C* **2021**, *9* (25), 7991–8001. <https://doi.org/10.1039/D1TC01751A>.
- (48) Huitorel, B.; Benito, Q.; Fargues, A.; Garcia, A.; Gacoin, T.; Boilot, J.-P.; Perruchas, S.; Camerel, F. Mechanochromic Luminescence and Liquid Crystallinity of Molecular Copper Clusters. *Chemistry of Materials* **2016**, *28* (22), 8190–8200. <https://doi.org/10.1021/acs.chemmater.6b03002>.
- (49) Dardel, B.; Guillon, D.; Heinrich, B.; Deschenaux, R. Fullerene-Containing Liquid-Crystalline Dendrimers. *J. Mater. Chem.* **2001**, *11* (11), 2814–2831. <https://doi.org/10.1039/B103798F>.

- (50) M. J. Frisch and G. W. Trucks and H. B. Schlegel and G. E. Scuseria and M. A. Robb and J. R. Cheeseman and G. Scalmani and V. Barone and G. A. Petersson and H. Nakatsuji and X. Li and M. Caricato and A. V. Marenich and J. Bloino and B. G. Janesko and R. Gomperts and B. Mennucci and H. P. Hratchian and J. V. Ortiz and A. F. Izmaylov and J. L. Sonnenberg and D. Williams-Young and F. Ding and F. Lipparini and F. Egidi and J. Goings and B. Peng and A. Petrone and T. Henderson and D. Ranasinghe and V. G. Zakrzewski and J. Gao and N. Rega and G. Zheng and W. Liang and M. Hada and M. Ehara and K. Toyota and R. Fukuda and J. Hasegawa and M. Ishida and T. Nakajima and Y. Honda and O. Kitao and H. Nakai and T. Vreven and K. Throssell and Montgomery, {Jr.}, J. A. and J. E. Peralta and F. Ogliaro and M. J. Bearpark and J. J. Heyd and E. N. Brothers and K. N. Kudin and V. N. Staroverov and T. A. Keith and R. Kobayashi and J. Normand and K. Raghavachari and A. P. Rendell and J. C. Burant and S. S. Iyengar and J. Tomasi and M. Cossi and J. M. Millam and M. Klene and C. Adamo and R. Cammi and J. W. Ochterski and R. L. Martin and K. Morokuma and O. Farkas and J. B. Foresman and D. J. Fox. *Gaussian 16, Revision A.03*; Gaussian, Inc., Wallingford CT, 2016.; 2016.
- (51) Licari, D.; Baiardi, A.; Biczysko, M.; Egidi, F.; Latouche, C.; Barone, V. Implementation of a Graphical User Interface for the Virtual Multifrequency Spectrometer: The VMS-Draw Tool. *Journal of Computational Chemistry* **2015**, *36* (5), 321–334. <https://doi.org/10.1002/jcc.23785>.
- (52) Huitorel, B.; El Moll, H.; Utrera-Melero, R.; Cordier, M.; Fargues, A.; Garcia, A.; Massuyeau, F.; Martineau-Corcós, C.; Fayon, F.; Rakhmatullin, A.; Kahlal, S.; Saillard, J.-Y.; Gacoin, T.; Perruchas, S. Evaluation of Ligands Effect on the Photophysical Properties of Copper Iodide Clusters. *Inorg. Chem.* **2018**, *57* (8), 4328–4339. <https://doi.org/10.1021/acs.inorgchem.7b03160>.
- (53) Thefioux, Y.; Cordier, M.; Massuyeau, F.; Latouche, C.; Martineau-Corcós, C.; Perruchas, S. Polymorphic Copper Iodide Anions: Luminescence Thermochromism and Mechanochromism of (PPh₄)₂[Cu₂I₄]. *Inorg. Chem.* **2020**, *59* (8), 5768–5780. <https://doi.org/10.1021/acs.inorgchem.0c00560>.
- (54) *CSD Cambridge Data Base*; 2021.
- (55) Ikeda, Tomiki.; Kurihara, Seiji.; Tazuke, Shigeo. Excimer Formation Kinetics in Liquid-Crystalline Alkylcyanobiphenyls. *J. Phys. Chem.* **1990**, *94* (17), 6550–6555. <https://doi.org/10.1021/j100380a008>.
- (56) Piryatinskiĭ, Yu. P.; Yaroshchuk, O. V. Photoluminescence of Pentyl-Cyanobiphenyl in Liquid-Crystal and Solid-Crystal States. *Opt. Spectrosc.* **2000**, *89* (6), 860–866. <https://doi.org/10.1134/1.1335034>.
- (57) Bezrodna, T.; Melnyk, V.; Vorobjev, V.; Puchkovska, G. Low-Temperature Photoluminescence of 5CB Liquid Crystal. *Journal of Luminescence* **2010**, *130* (7), 1134–1141. <https://doi.org/10.1016/j.jlumin.2010.02.009>.
- (58) Shah, A.; Sannaikar, M. S.; Inamdar, S. R.; Duponchel, B.; Douali, R.; Singh, D. P. Photoluminescence Modulation in the Graphene Oxide Dispersed 4-n-Octyl-4'-Cyanobiphenyl Molecular System. *Journal of Luminescence* **2020**, *226*, 117509. <https://doi.org/10.1016/j.jlumin.2020.117509>.
- (59) Nagai, K.; Utsunomiya, K.; Takamiya, N.; Nemoto, N.; Kaneko, M. Photoluminescence of Polysiloxane Containing Mesogenic 4-Cyanobiphenyl in Solution. *Journal of Polymer Science Part B: Polymer Physics* **1996**, *34* (12), 2059–2065. [https://doi.org/10.1002/\(SICI\)1099-0488\(19960915\)34:12<2059::AID-POLB11>3.0.CO;2-0](https://doi.org/10.1002/(SICI)1099-0488(19960915)34:12<2059::AID-POLB11>3.0.CO;2-0).
- (60) Teunissen, A. J. P.; Pérez-Medina, C.; Meijerink, A.; Mulder, W. J. M. Investigating Supramolecular Systems Using Förster Resonance Energy Transfer. *Chem. Soc. Rev.* **2018**, *47* (18), 7027–7044. <https://doi.org/10.1039/C8CS00278A>.
- (61) Jiang, N.; Wang, R.; You, X.; Geng, Y.; Zhu, D.; Zhang, N.; Bryce, M. Supramolecular Oligourethane Gels as Light-Harvesting Antennae: Achieving Multicolour Luminescence and White-Light Emission through FRET. *J. Mater. Chem. C* **2021**, *9* (38), 13331–13337. <https://doi.org/10.1039/D1TC03105H>.